



Additive Manufacturing and Performance of Architected Cement-Based Materials

Moini, M., Olek, J., Youngblood, J., Magee, B., & Zavattieri, P. (2018). Additive Manufacturing and Performance of Architected Cement-Based Materials. *Advanced Materials*, 30(43), 1-11. Article 1802123.
<https://doi.org/10.1002/adma.201802123>

[Link to publication record in Ulster University Research Portal](#)

Published in:
Advanced Materials

Publication Status:
Published (in print/issue): 22/10/2018

DOI:
[10.1002/adma.201802123](https://doi.org/10.1002/adma.201802123)

Document Version
Author Accepted version

General rights

The copyright and moral rights to the output are retained by the output author(s), unless otherwise stated by the document licence.

Unless otherwise stated, users are permitted to download a copy of the output for personal study or non-commercial research and are permitted to freely distribute the URL of the output. They are not permitted to alter, reproduce, distribute or make any commercial use of the output without obtaining the permission of the author(s).

If the document is licenced under Creative Commons, the rights of users of the documents can be found at <https://creativecommons.org/share-your-work/licenses/>.

Take down policy

The Research Portal is Ulster University's institutional repository that provides access to Ulster's research outputs. Every effort has been made to ensure that content in the Research Portal does not infringe any person's rights, or applicable UK laws. If you discover content in the Research Portal that you believe breaches copyright or violates any law, please contact pure-support@ulster.ac.uk

Advanced Materials

Additive Manufacturing and Performance of Architected Cement-based Materials --Manuscript Draft--

Manuscript Number:	
Full Title:	Additive Manufacturing and Performance of Architected Cement-based Materials
Article Type:	Communication
Section/Category:	
Keywords:	direct ink writing, architected material, hardened cement paste, interface, mechanical response, bioinspired materials
Corresponding Author:	Pablo Zavattieri Purdue University West Lafayette, IN UNITED STATES
Additional Information:	
Question	Response
Please submit a plain text version of your cover letter here. If you are submitting a revision of your manuscript, please do not overwrite your original cover letter. There is an opportunity for you to provide your responses to the reviewers later; please do not add them here.	Dear Dr. Lenders, We wish to submit the paper entitled "Additive Manufacturing and Performance of Architected Cement-based Materials" for publication in the Advanced Materials. There is a quest to use additive manufacturing for 3D printing cementitious materials. However, due to the intrinsic limited strength, brittle behavior and presence of weak interfaces, this is a very challenging task. In this article, we examine the use of bioinspired architectures to create 3D printing cementitious materials with improved mechanical properties. In our work, we demonstrate that using bioinspired architectures with clever mechanisms that prevent catastrophic failure, we are able to increase the fracture energy by more than 150% with respect to its base material without sacrificing the strength of the base materials (similar to what we also find in natural materials). We believe that this article fits into the scope of Advanced Materials as it brings important information about the role of architecture in materials. It shows controlled spread of damage through relatively weak interfaces, which is counter-intuitive in brittle materials. It also brings new insights into materials design. This is important considering that several current research efforts are actually trying to eliminate these interfaces. Please do not hesitate to contact me should you have any questions. Sincerely, Pablo Zavattieri Purdue University
Do you or any of your co-authors have a conflict of interest to declare?	No. The authors declare no conflict of interest.
Corresponding Author Secondary Information:	
Corresponding Author's Institution:	Purdue University
Corresponding Author's Secondary Institution:	
First Author:	Mohamadreza Moini
First Author Secondary Information:	
Order of Authors:	Mohamadreza Moini Jan Olek, PhD Jeffrey Youngblood, PhD Bryan Magee, PhD

	Pablo Zavattieri
Order of Authors Secondary Information:	
Abstract:	<p>There is an increasing interest in Additive Manufacturing (AM) applied to cement-based materials. However, the intrinsic brittle behavior of these materials and the presence of interfaces from the additive manufacturing process represent the current major challenges. Contrary to what most research groups are doing to eliminate interfaces and add reinforcement, our work focuses on harnessing the role of relatively weak interfaces by employing clever design guidelines from bio-inspired architected materials. These architectures play a significant role in enabling novel performance characteristics, such as toughening, spread of damage and flaw-tolerance. The control of the architecture of cement paste materials through AM allows initiation and propagation of micro-cracking at key locations in the layered structures, and can play a role in tuning, enhancing and diversifying the mechanisms that improve work of fracture, strength, and inelastic deflection of the structure. Evidence is provided by multiaxial flexural tests comparing the architected materials with cast specimens. We observe that these architectures can significantly depart from the typical strength-porosity relationship, classically known for brittle materials. In turns, these architectures show improvements of the work of fracture by more than 150% exhibiting controlled spread of damage without sacrificing strength.</p>

1
2
3
4 DOI: 10.1002/((please add manuscript number))

5 **Article type: Communication**
6
7

8
9
10 **Additive Manufacturing and Performance of Architected Cement-based Materials**
11

12
13
14 *Mohamadreza Moini, Jan Olek, Jeffrey Youngblood, Bryan Magee, Pablo D. Zavattieri**
15

16
17
18 M. Moini, Prof. J. Olek, Prof. P. D. Zavattieri
19

20
21 Lyles School of Civil Engineering, Purdue University at West Lafayette, Indiana 47907, USA
22

23
24 E-mail: zavattie@purdue.edu
25

26
27 Prof. J. Youngblood
28

29
30 School of Materials Engineering, Purdue University at West Lafayette, Indiana 47907, USA
31

32
33 Dr. Bryan Magee
34

35
36 Built Environment Research Institute, Ulster University at Newtownabbey, BT37 0QB, UK
37

38
39 Keywords: direct ink writing, architected material, hardened cement paste, interface,
40
41 mechanical response
42
43
44
45
46
47
48
49
50
51
52
53
54
55
56

1
2
3
4 Abstract:
5

6
7 There is an increasing interest in Additive Manufacturing (AM) applied to cement-based
8
9 materials. However, the intrinsic brittle behavior of these materials and the presence of
10
11 interfaces from the additive manufacturing process represent the current major challenges.
12
13 Contrary to what most research groups are doing to eliminate interfaces and add
14
15 reinforcement, our work focuses on harnessing the role of relatively weak interfaces by
16
17 employing clever design guidelines from bio-inspired architected materials. These
18
19 architectures play a significant role in enabling novel performance characteristics, such as
20
21 toughening, spread of damage and flaw-tolerance. The control of the architecture of cement
22
23 paste materials through AM allows initiation and propagation of micro-cracking at key
24
25 locations in the layered structures, and can play a role in tuning, enhancing and diversifying
26
27 the mechanisms that improve work of fracture, strength, and inelastic deflection of the
28
29 structure. Evidence is provided by multiaxial flexural tests comparing the architected
30
31 materials with cast specimens. We observe that these architectures can significantly depart
32
33 from the typical strength-porosity relationship, classically known for brittle materials. In
34
35 turns, these architectures show improvements of the work of fracture by more than 150%
36
37 exhibiting controlled spread of damage without sacrificing strength.
38
39
40
41
42
43
44
45
46
47
48
49
50
51
52
53
54
55
56
57
58
59
60
61
62
63
64
65

1
2
3
4 There is a rising interest in hierarchical design and additive manufacturing (AM) of
5
6 architected materials due to their ability to achieve unique and novel performance
7
8 characteristics ^[1-8]. The AM allows for fabrication of complex solid and cellular structures,
9
10 and thus enables numerous opportunities for generation of novel, and unconventional
11
12 behaviors via controlled mechanical responses, or enhanced properties ^[9-12].
13
14

15
16
17 The focus of this work is on 3D printing of brittle cement-based materials, in which the ability
18
19 to control the internal architecture of the structure at the macroscopic (i.e. mm scale) may play
20
21 a significant role by enabling novel performance characteristics, such as a quasi-brittle
22
23 mechanical behavior, fracture and damage tolerance, unique load-displacement response, and
24
25 enhanced flexural strength. The control of the architecture of materials through AM alters the
26
27 crack propagation at the interface in layered bioinspired structures, and can play a role in
28
29 tuning, enhancing and diversifying the mechanical response and toughening mechanisms ^{[13-}
30
31 ^{19]}. Materials with such enhanced properties may impact design approaches, processes, and
32
33 products in several industries ^[20,21].
34
35
36

37
38
39 Despite recent works on processing ^[22-24] and mechanical properties of 3D printed cement-
40
41 based materials ^[25-30], as well as earlier works on microstructural aspects of fracture properties
42
43 of cast cement paste ^[31-33], there are only limited studies that highlight control of the
44
45 mechanical behavior through the architecture of cement-based materials ^[34,35]. Because the
46
47 presence of weak interface is considered detrimental for the overall mechanical performance
48
49 of cementitious materials, current research efforts focus mostly on eliminating or
50
51 strengthening AM-induced interfaces as a mean to minimize their effect on the overall
52
53
54
55
56

1
2
3
4 strength, bearing capacity and improve stress transfer across or the interfaces in certain
5 direction in 3D printed elements [26-30]. Contrary to that line of research, our work attempts to
6 harness these relatively weak interfaces by examining the role of the architecture as a mean of
7 controlling and diversifying the mechanical response of brittle cement paste elements.
8
9

10
11
12
13
14 Due to its intrinsic properties, the cast hardened cement paste (hcp) does not exhibit typical
15 toughening mechanisms, e.g. crack branching, observed in other materials [36,37].
16 Correspondingly, cast cement paste behaves as brittle material and does not show non-linear
17 behavior [38]. However, existing studies demonstrated that directionality of response, as
18 enabled by controlling the internal architecture of the elements, can play a part in spreading of
19 the damage, and may improve overall inelastic response of composite materials, specifically
20 brittle ceramics and compliant organics [13-18]. In this work, the mechanical response of 3D
21 printed cement paste elements with specific architectures, along with the associated damage
22 mechanisms, have been investigated by examining the behavior of both, the individual
23 filaments (i.e. layered deposited material) and the interfaces between the filaments.
24
25
26
27
28
29
30
31
32
33
34
35
36
37
38

39
40 Many of the internal architectures, that can be fabricated via 3D printing are not attainable, or
41 are extremely challenging to achieve, using conventional casting methods. To illustrate this
42 point, we present several elements with variable architectures achieved by 3D-printing of the
43 ordinary portland cement paste using the direct-ink-writing (DIW) method. These
44 architectures included: a closed cell honeycomb pattern (**Figure 1a**), a ‘Bouligand’
45 architecture with helicoidal alignment of filaments at pitch angles $\gamma = 2^\circ$ and 45° , (**Figures**
46
47
48
49
50
51
52
53
54
55
56
57
58
59
60
61
62
63
64
65

1
2
3
4 **1b,c)**, a grid architecture (**Figure 1d**), a cellular sandwich panel prism with solid top and
5
6 bottom layers (**Figure 1e**), and a compliant structure with honeycomb pattern (**Figure 1f**).

7
8
9
10 When subjected to cycling loading, a compliant structure with honeycomb pattern (similar to
11
12 that illustrated in **Figure 1f**) displayed bi-linear stress-strain behavior characterized by two
13
14 discrete values of moduli of elasticity (see Figure S1 in supporting materials).

15
16
17 The values of modulus of rupture (MOR) of printed solid prisms with various filament
18
19 orientations (i.e., 0°, 45°, and 90° with respect to X-axis) were determined using the three-
20
21 point-bending (3PB) test (**Figure 2a**). A comparison of average values of specific MOR for
22
23 printed and cast specimens (**Figure 2c**) reveals that they were not statistically different (i.e.,
24
25 $p \geq 0.05$ for all printing angles versus cast). This implies that the mechanical response of all
26
27 three of the printed prisms was independent of the orientation of the filament and the
28
29 specimen processing method (i.e. printed vs. cast). Since there has been observable difference
30
31 in the crack patterns as function of filament orientation (**Figure 2d-m**), the lack of statistically
32
33 discernible difference in the values of specific MOR (in spite of the trends in strength between
34
35 printed and cast specimen in **Figure 3c**) may simply imply that the 3PB test is not capable to
36
37 adequately capture the microscopic level fracture response.

38
39
40 Previous research, indicated that 3D-printed cement-based elements exhibited zones of
41
42 weakness at the interfaces between individual filaments^[26-30], a phenomenon not commonly
43
44 observed in conventionally cast prisms. The influence of pronounced interfaces on the overall
45
46 crack path, and on the associated micro-cracking, has been observed to be unique for each of
47
48 the 0° and 45° architectures used in this study. Specifically, the crack path in two types of the
49
50
51
52
53
54
55
56

1
2
3
4 tested prisms (i.e. those with 0° and 45°) intercepted the filaments (**Figures 2d,e**) whereas the
5
6 crack path was parallel to the filament in the third type of the prism (i.e. the one with 90°
7
8 architecture). When the first two types of prisms (i.e. 0° and 45°) were examined in XZ plane
9
10 microscopically, the crack path was observed to partially deflected to a potentially weak
11
12 interface along the layered filaments (parallel to the X direction), resulting in a staggered
13
14 crack pattern (**Figures 2g,h**). Furthermore, examination of **Figure 2j,k**, reveals that at the
15
16 locations where the crack is being deflected along the filament (i.e. in the X-direction) there is
17
18 an accompanying development of micro-cracking that spreads along the interface between the
19
20 two filament. In contrast, for the prisms with 90° orientation, only a single, predominantly
21
22 unidirectional crack is developed along one of the interfaces (**Figure 2i**). Additionally, no
23
24 micro-cracking was observed.
25
26
27
28
29
30

31
32 For 90° prisms, we can infer that the overall crack localized at the interface with no crack
33
34 deflection and micro-cracking advancing into the interface (**Figures 2f,i,m**). Overall,
35
36 examination of the crack paths in these three architectures indicates a potential weak interface
37
38 in 3D printed elements. The demonstrated crack paths in all three architectures suggest that
39
40 controlling the architecture of solid prism (via varying filament orientation) can be used to
41
42 control the crack path in solid 3D printed prisms. The micro-cracking at the point of crack
43
44 deflection indicates that the interface can be utilized to introduce a mechanism for micro-
45
46 crack propagation solid structures and allow for a new damage behavior uncommon in cast
47
48 elements.
49
50
51
52
53
54
55
56
57
58
59
60
61
62
63
64
65

1
2
3
4 The Bouligand architectures utilized here have found applications in engineering materials
5 and offer increased toughness and energy absorption by enabling crack propagation in a
6
7 stepwise pattern, crack redirection, branching, and prevention of catastrophic failure in
8
9 various biological organisms ^[39,40]. Moreover, previous investigations have shown that
10
11 Bouligand architectures, such as those found in the endocuticles of arthropods, tend to grow
12
13 cracks in twisted patterns following the direction of the fiber ^[39]. These twisting patterns have
14
15 been found to be responsible for increasing toughness ^[41] and promote spread of damage ^[48].
16
17 To further investigate the architecture-performance relationship, Bouligand architectures
18
19 printed with several pitch angles ($\gamma = 8^\circ, 15^\circ, 30^\circ, 45^\circ, 90^\circ$) and infill percentage (60% to
20
21 100%) are studied for specific strength, and work of fracture (WOF), and load-displacement
22
23 behavior, and compared with conventionally cast structures (**Figure 3a**). The Bouligand
24
25 architecture demonstrated consistently higher degrees of deflection compared to cast
26
27 structures. This additional degree of deflection is uncommon in brittle materials and is
28
29 reflected in **Figure 3a** by 105%, 125%, and 150% for architectures with $\gamma = 8^\circ$ (60% infill), γ
30
31 = 45° (60% infill), and $\gamma = 8^\circ$ (solid), respectively. It must be noted that these cellular and
32
33 solid structures have achieved higher deflection while having relative densities (i.e. density of
34
35 each specimen relative to the average of the conventional cast solid controls) lower than cast
36
37 specimens (as low as 0.5).
38
39
40
41
42
43
44
45
46
47
48

49 As discussed in prism study above, the deflection of the crack path into the interface and
50
51 presence of micro-cracks in the interfaces is also of particular importance for the printed disc
52
53 structures. These two features in the Bouligand architectures can enable the spread of the
54
55
56
57
58
59
60
61
62
63
64
65

1
2
3
4 damage in the structure by localization of micro-cracks and fracture of sacrificial links
5
6 without sacrificing the integrity of the structure. The damage and fracture of filaments at pre-
7
8 and post-peak is additionally captured. The screen shot of the acoustic recording of the
9
10 fracture during testing for $\gamma = 45^\circ$ and cast control is also illustrated in **Figure 3a**. The screen
11
12 shot of the acoustic recordings qualitatively describe the propagation of multiple cracks prior-
13
14 and post-peak in the Bouligand structure is distinguished when compared to fracture of cast
15
16 cement in a brittle manner (**Figure 3a**). The major peaks of the acoustic graph match the local
17
18 maximum loads.
19
20
21
22
23

24 In terms of specific properties, the majority of Bouligand structures ($\gamma = 15^\circ, 30^\circ, 45^\circ, 90^\circ$),
25
26 other than $\gamma = 8^\circ$ with 60% infill, are statistically similar in average specific MOR when
27
28 compared to cast structures (**Figure 3b**). This equivalent performance includes small pitch
29
30 angle with $\gamma = 8^\circ$ with 100% infill (i.e., solid).
31
32
33
34

35 The WOF is assessed for all Bouligand architectures, and an increase in WOF is observed as γ
36
37 increased from 8° to 90° for 60% infill structures (**Figure 3c**), with highest WOF in $\gamma = 90^\circ$.
38
39 The observed pattern is consistent with previous studies on composite materials with the
40
41 Bouligand structure, suggesting increased WOF with increase in rotation angle ^[33]. **Figure 3c**
42
43 describes how γ or infill percentage can play a role in the fracture properties of materials. The
44
45 solid structures with $\gamma = 8^\circ$, however, demonstrated elevated WOF compared to its identical
46
47 γ at lower density (60% infill). This is in accordance with what is observed in similar
48
49 Bouligand structures in relation to pitch angle ^[40]. The solid structures with $\gamma = 8^\circ$ show a
50
51 counter-clock-wise orientation of the fractured plane following the right-hand pattern in
52
53
54
55
56
57
58
59
60
61
62
63
64
65

1
2
3
4 consecutive layers (positive counter-clock-wise γ). This Bouligand study demonstrates the
5
6 ability to control the WOF by controlling the pitch angle and relative density in brittle
7
8 materials.
9

10
11 The performance of Bouligand structures in terms of MOR with respect to their relative
12
13 density is assessed for various γ and compared to conventionally cast ‘cellular solid’ over a
14
15 broad range of porosity (**Figure 3d**). Apparent from **Figure 3d**, and benchmarked against
16
17 theoretical curve and values of MOR for hardened cast cellular cement paste ^[43], is the
18
19 emergence of a distinct group of printed Bouligand architectures with $\gamma = 15-90^\circ$ (shown as a
20
21 blue region in **Figure 3d**) that consistently out-performs conventionally cast specimens across
22
23 the relative density range considered (0.5-0.65). This presents clear indication that higher
24
25 performance is attainable by 3D printed Bouligand architectures relative to conventionally
26
27 cast controls with equivalent density, reflecting the unique ability of specimen architecture to
28
29 control mechanical response. Conversely, less favourable performance in terms of MOR was
30
31 noted for the 60% infill, $\gamma = 8^\circ$ specimens (**Figures 3d**).
32
33
34
35
36
37
38
39

40 Bouligand architectures are further studied for identification of fracture patterns, crack-paths,
41
42 and micro-cracks using optical microscopy (**Figure 4**). A variety of fracture paths and crack
43
44 patterns are exhibited at the bottoms (**Figures 4a.1-c.1**) and cross-sections of Bouligand
45
46 architectures (**Figures 4a.2-c.2**). In $\gamma = 45^\circ$ with 60% infill, the crack path appear to shear the
47
48 filaments (**Figure 4a.1**), whereas it occurred at the interface between adjacent filaments in 8°
49
50 with 60% infill and in solid structure with 100% infill (**Figures 4a.2,a.3**). The crack path, for
51
52 the $\gamma = 45^\circ$, typical in Bouligand structures resulted in shear failure in filaments with a certain
53
54
55
56

1
2
3
4 orientation, whereas the filaments in the layers parallel to the main failure plain remained
5 intact (in layer 1- bottom and layer 5, **Figures 4c.3**). In contrast, with **Figures 4c.3**, horizontal
6 propagation of crack paths at the interface is also observed at $\gamma = 8^\circ$ structures with 60% infill
7 (layer 4 and 5) as demonstrated in **Figures 4b.3,b.4**. In the solid structures with $\gamma = 8^\circ$, the
8 crack propagates at the interface between layers 6 and 7 throughout the cross-section and
9 between layers 2 and 3 near the crack divergence points (**Figure 4a.3**). In addition, a
10 staggered fractured pattern is observed in the main failure plane (**Figure 4a.8**).

11
12 Advancement of the micro-crack at the interface in solid $\gamma = 8^\circ$ category is further observed
13 with multiple parallel micro-cracking throughout the cross section (**Figure 4a.3**) and at the
14 bottom and top layer (**Figures 4a.4,a.5,a.6**). The higher WOF for solid structures with $\gamma = 8^\circ$
15 seemed higher than that for structures with 60% infill and $\gamma = 8^\circ$ and 45° , and the
16 conventionally cast discs (**Figure 3c**), may be attributed to the allowance of micro-crack
17 advancement at the interface and may allow for the higher deflection at failure as discussed
18 previously (**Figure 3a**).

19
20 Micro-cracking in different arrangements and in bridging elements between the filaments in
21 Bouligand architectures are also recognized in $\gamma = 30^\circ$ structures. Multiple parallel micro-
22 cracks near the fractured face of specimens at the bottom layers 1, 2 and 3 is observed
23 (**Figures 4d.1,d.2**). These parallel micro-cracks are spaced equally from the fracture edge in
24 the very bottom layer (**Figure 4d.1**) and appear twisting in the subsequent bottom layers 2 and
25 3 and at the bridging link (**Figure 4d.2**). These patterns are consistent with what was found in
26 other in similar biomimetic Bouligand composite materials ^[42].

1
2
3
4 A similar sinusoidal fractured pattern is observed in both categories of Bouligand
5 architectures, the 8° with 60% infill and solid 100% infill (**Figures 4a.7,b.5**). This pattern is
6
7 repeated in solid 8° specimens between layers 6 and 7 and between layers 2 and 3 and is
8
9 viewed in cross section (**Figure 4a.3**), whereas it is observed throughout the elevation view of
10
11 8° with 60% infill (**Figure 4b.5**). In the former, it is noteworthy that there is an intra-layer
12
13 sinusoidal pattern between consecutive layers due to small γ (8°) and a subsequent pattern
14
15 offset associated with the small angle orientation (**Figure 4a.7**), and in the later it is
16
17 noteworthy that the micro-crack advancement is observed in the interface similar to other
18
19 categories (**Figure 4b.6**).

20
21 Overall, in Bouligand architectures, the crack deflection at the interface is commonly
22
23 observed in smaller categories of γ (8° with 60% infill and 100% solid, **Figures 4b.3,b.4,a.1**).

24
25 The micro-crack advancement at the interface is also observed in various architectures
26
27 (**Figures 5a.3-a.6,b.5**) indicating weaker properties at the interface. The presence of this weak
28
29 interface, not only allows to control the crack path to follow the interface, but also can initiate
30
31 numerous micro-crack advancement. Acknowledging this possibility, various architectures
32
33 can then be tailored for the anticipated crack at the interface to follow a desirable pattern, and
34
35 may provide an increased threshold to crack initiation, initiation toughness, and WOF (**Figure**
36
37 **3c**).

38
39 The fracture behavior of cast cement, commonly exhibits brittle and unstable crack
40
41 propagation ^[30]. Overall, in 0° and 45° architectures in solid prism, horizontal deflection of
42
43 crack is demonstrated and redirected at the interface, followed by advancement of micro-

1
2
3
4 cracks at the interface between filaments (**Figures 2g,h**). This crack deflection and the
5
6 subsequent micro-crack induction, suggests the possibility of increased spread of the damage
7
8 in design of these architected materials. In 90° prisms, no micro-crack or crack deflection at
9
10 the interface is observed. However, a remarkable observation in this case is that the main
11
12 crack occurs at the interface between the filaments in the mid-span of the specimen in the
13
14 entire cross section (**Figures 3h**). This indicates the presence of interface with specific
15
16 interfacial strength, distinguished from intra-filament in 3D printed prisms. The demonstrated
17
18 interface between layers can be utilized in an architecture in which micro-cracks can be
19
20 advanced in multi-layers and allow for an intrinsic fracture toughening mechanism ^[13,14].
21
22
23
24
25

26
27 More broadly, in both types of solid prisms and Bouligand architectures studied in this work,
28
29 micro-crack advancement along the interface is observed. In most cases, the initiated micro-
30
31 cracks in solid prisms (**Figure 2g,h**) and solid Bouligand structures (**Figures 4a.3-a.6**) spread
32
33 all the way to the edge of the prism and disc. Moreover, these interfacial micro-cracks are
34
35 straight on a macroscopic scale, and follow the architectural pattern of the interfaces, both in
36
37 prism (**Figures 2g,h**) and Bouligand architectures. Typical fracture features of brittle cement
38
39 initiated from Knoop dent, for example, is discussed to have a macroscopic scale (merely 0.5
40
41 to 5 mm for a 3-kg indentation load) and extend straight along the dent, followed by forward
42
43 and backward crack branches on the order of 10s of microns and a common termination in a
44
45 short fork form ^[36]. In contrast, we demonstrate that the properties of the interface between
46
47 the filaments can be designed to act as a crack trap leading to prompt multiple site nucleation
48
49 across filaments, and eventually define the overall response of the materials in 3D printed
50
51 architectures under loading.
52
53
54
55
56

1
2
3
4 The periodic crack patterns found in bridging elements near the failure plain in the 30°
5
6 Bouligand architecture signifies that architecture of a material can allow for induction of
7
8 cracks through sacrificial links without compromising the integrity of the structure. The
9
10 failure of sacrificial links does not necessarily decrease the strength (**Figure 3b**), however it
11
12 can contribute to the spread the damage due to improved initiation toughness ^[14]. Such
13
14 architectures, in spite of the brittle nature of their base materials, can undertake localized
15
16 damage triggered by sacrificial links (**Figures 4d.1,d.2**) and yet be able to tolerate micro-
17
18 cracks in each link. These micro-cracks can contribute to overall inelastic deformation and
19
20 toughening of the material without abrupt macroscopic failure of the structure. Further
21
22 understanding of such systems, can result in design of flaw-tolerant brittle architected
23
24 materials such as hardened cement paste. Practically, the growth of the micro-cracks
25
26 throughout the structure avoids the localization of micro-cracks and allows multiple micro-
27
28 crack propagation at the interface such as those observed in prisms and Bouligand
29
30 architectures.

31
32
33
34
35
36
37
38 In summary, this work presents the role of the architecture of the materials by exploring bio-
39
40 inspired design and heterogeneities induced by the interfaces as a mean of controlling and
41
42 diversifying the mechanical response of brittle cement paste elements. we have demonstrated
43
44 that architecture of the structure can uncover novel behaviors of cementitious materials via
45
46 DIW process. These behaviors, observed in compliant design (see supporting information),
47
48 prism and Bouligand architectures, demonstrate new capacities to engineering performance of
49
50 cementitious materials. Architectures such as compliant design demonstrated bilinear stress-
51
52 strain behavior, not attainable in cast elements, and provides the ability to customize stress-
53
54
55
56
57
58
59
60
61
62
63
64
65

1
2
3
4 strain behavior as applicable. In prism type structures, using architecture to control the crack
5 path and allow advancement of multi micro-cracking (and spread of the damage) using an
6
7 intrinsic fracture toughening mechanism is conceivable. Processing-induced weak interfaces
8
9 are commonly considered defects in cementitious materials and are avoided. In Bouligand
10
11 architectures, we demonstrated that such heterogeneities interfaces exist and are not
12
13 necessarily detrimental to the overall performance, but also can provide mechanisms that can
14
15 lead to novel responses such as an increased deflection in load-displacement, increased WOF,
16
17 and other properties unimagined for hardened cement paste materials. In addition, the
18
19 viability of deflecting the crack path at the interface and initiating micro-cracks through the
20
21 interface, offers new possibilities in spread and control of the damage, in fracture
22
23 mechanisms, and in hierarchical design of materials. To further explore opportunities
24
25 provided by architected cement paste materials, a fundamental understanding on the
26
27 intertwined relationships between processing-induced heterogeneities, ink properties (cement
28
29 hydration, rheology, chemistry, and formulation), architectural parameters (such as pitch
30
31 angle and infill percentage), and microstructural characteristics of the intra-filaments and
32
33 inter-filaments (interfaces) must be developed to fine tune the performance of resulting
34
35 elements. Further understanding of the architectural parameters, can result in design of flaw-
36
37 tolerant architected materials with brittle base such as hardened cement paste.
38
39
40
41
42
43
44
45
46
47

48 **Experimental Section:**

49
50
51 *Cementitious Ink Formulation:* An iterative trial and error ink design procedure is used to
52
53 identify cement inks suitable for DIW process. The ink with proper flow properties that can
54
55
56

1
2
3
4 overcome processing challenges such as flocculation, bleeding, and can result in suitable
5
6 shape holding is designed. The final ink used constituted the sub 150 μm fraction of
7
8 commercially available Type I cement (Buzzi Unicem USA) in accordance with ASTM C150
9
10 [44], deionized water, and both high range water reducing admixture (HRWRA-
11
12 MasterGlenium 7700) and viscosity modifying admixtures (VMA-MasterMatrix 362) in
13
14 accordance with ASTM C494 [45] and the findings of previous study [46]. For each 250 g of
15
16 cement, the mix comprised 65.2, 1.1 and 3 g of deionized water, HRWRA and VMA,
17
18 respectively.
19
20
21
22
23

24 *Mixing Procedure:* A Twister Evolution Venturi vacuum mixer is used in three steps to mix
25
26 and eliminate entrapped air. Admixtures are added and dispersed in water and mixed with
27
28 cement at 400 rpm for 25 s, at 400 rpm for 90 seconds at 70% vacuum and then finally at
29
30 400rpm at 100% vacuum.
31
32
33

34 *3D Printing:* A bespoke system is developed by merging a 3D printer typically used for
35
36 printing thermoplastics (Ultimaker 2 Extended+) with a stepper motor-driven extrusion
37
38 system (Structur3d Discov3ry Paste Extruder) capable of applying desirable extrusion rates to
39
40 mounted 75 mL ink-charged syringes. The 3D printer hardware is modified by mounting a
41
42 lightweight aluminium nozzle holder on the gantry for nozzle placement. The printer and
43
44 extrusion system are merged through standard luer locks and polyethylene tubing. A nozzle
45
46 with an internal diameter of 1.36 mm is used. Slicer-generated g-code command included X,Y,
47
48 Z point cloud coordinates and E (extrusion), and F (printing speed) axis movement commands
49
50 specific to each design. A 1 mm layer height and 250 mm/min printing speed is used
51
52
53
54
55
56
57
58
59
60
61
62
63
64
65

1
2
3
4 throughout. Specimens are transferred to a curing chamber with relative humidity of $93.58 \pm$
5
6
7 0.66 % (using potassium nitrate) at 25 °C immediately after printing or casting.
8

9
10 *Characterization:* Flexural strength and modulus-of-rupture (MOR), is used to characterize
11
12 the mechanical properties via uniaxial three-point bending (3PB) testing of prism specimens
13
14 and multi-axial ball-on-three-ball (B3B) testing of disc-shaped specimens. For 3PB testing,
15
16 prisms are designed to have final dimensions of 12 x 12 x 40 mm, with surfaces being ground
17
18 flat prior to testing to ensure acceptable tolerances and good contact with test support plates
19
20
21
22 ^[47]. MOR is calculated based on the measured dimensions of each specimen. B3B testing is
23
24 adopted given its high sensitivity to internal defects and insensitivity to outer and surface
25
26 imperfections ^[48,49]. A load is applied via a central ball on the top face of round, disc-shaped
27
28 specimen of 55 mm diameter and 8 mm thickness supported underneath by three equally sized,
29
30 equidistantly spaced balls placed on a circle of diameter of 50 mm ^[50]. Bouligand structure
31
32 discs are aligned to ensure that bottom filament orientation is aligned with the minimum stress
33
34 field. A stereo microphone device (Zoom iQ6) with customizable stereo width is used to
35
36
37 capture crack noise.
38
39

40
41
42 Force and displacement for both tests are measured using a 10 kN capacity test rig (MTS
43
44 insight 10). All reported data is an average of at least two specimen results. Specimen relative
45
46 density is calculated from measured mass and volume of each specimen divided by the
47
48 average mass of conventionally cast ‘solid’ specimens. Specific MOR is calculated by
49
50 dividing the MOR value for each specimen by its relative density. WOF is calculated by
51
52 integrating areas under load-displacement curves. Two theoretical relationships between
53
54
55
56

1
2
3
4 porosity and strength for brittle materials are presented in **Figure 4d** and describe the
5
6 strength-porosity relationship of lightweight cellular structures based on strength of a control
7
8 specimen with zero porosity ^[43,51,52]. All specimens are tested at the age of 3 days (72±2
9
10 hours). Aluminium powder and variations of water/cement ratios are used to cast lightweight
11
12 cellular specimens.
13
14

15 16 17 **Supporting Information**

18
19
20 Supporting Information is available from the Wiley Online Library or from the author.
21
22

23 **Acknowledgements**

24
25
26 The authors gratefully acknowledge generous support from the National Science Foundation
27
28 (CMMI 1562927) of this research. The authors would also like to thank the BASF chemicals
29
30 company for providing materials.
31
32
33
34
35
36

37 **References**

- 38
39
40 [1] U. G. Wegst, H. Bai, E. Saiz, A.P. Tomsia, R. O. Ritchie, *Nat. Mater.* **2015**, *14*, 23.
41
42 [2] E. B. Duoss, T.H. Weisgraber, K. Hearon, C. Zhu, W. Small, T.R. Metz, J.J. Vericella,
43
44 H. D. Barth, J.D. Kuntz, R. S. Maxwell, C.M. Spadaccini, *Adv. Funct. Mater.* **2014**, *24*, 4905.
45
46 [3] J. P. Lewicki, J. N. Rodriguez, C. Zhu, M.A. Worsley, A.S. Wu, Y. Kanarska, J.D.
47
48 Horn, E. B. Duoss, J. M. Ortega, W. Elmer, R. Hensleigh, **2017**, *Sci. Rep.* *7*, 43401.
49
50
51 [4] B. G. Compton, J. A. Lewis, *Adv. Mater.* **2014**, *26*, 5930.
52
53
54
55
56
57
58
59
60
61
62
63
64
65

- 1
2
3
4 [5] K. T. Sullivan, C. Zhu, E. B. Duoss, A. E. Gash, D. B. Kolesky, J. D. Kuntz, J.A.
5
6 Lewis, C.M. Spadaccini, *Adv. Mater.* **2016**, 28, 1934.
7
8
9 [6] A.S. Gladman, E.A. Matsumoto, R. G. Nuzzo, L. Mahadevan, J. A. Lewis, *Nat.*
10
11 *Mater.* **2016**, 15, 413.
12
13
14 [7] C. Gosselin, R. Duballet, P. Roux, N. Gaudillière, J. Dirrenberger, P. Morel, *Mater.*
15
16 *Des.* **2016**, 100, 102.
17
18
19 [8] NSF Workshop on Additive Manufacturing for Civil Infrastructure Design and
20
21 Construction, 2017, <https://events.tti.tamu.edu/conference/nsf-3dp-workshop/>
22
23
24 [9] Q. Zhang, X. Yang, P. Li, G. Huang, S. Feng, C. Shen, B. Han, X. Zhang, F. Jin, F.
25
26 Xu, T.J. Lu, *Prog. Mater. Sci.* **2015**, 74, 332.
27
28
29 [10] E. Munch, M.E. Launey, D.H. Alsem, E. Saiz, A.P. Tomsia, R.O. Ritchie, *Sci.* **2008**,
30
31 322, 1516.
32
33
34 [11] L.J. Gibson, M. F. Ashby. *Cellular solids: structure and properties*, Cambridge
35
36 university press, **1999**.
37
38
39 [12] S. W. Cranford, A. Tarakanova, N.M. Pugno, M.J. Buehler, *Nat.* **2012**, 482, 72.
40
41
42 [13] Y. Zhang, H. Yao, C. Ortiz, J. Xu, M. Dao, *J. Mech. Behav. Biomed. Mater.* **2012**, 15,
43
44 70.
45
46
47 [14] E. Lin, Y. Li, J.C. Weaver, C. Ortiz, M.C. Boyce, *J. of Mater. Res.* **2014**, 29, 1867.
48
49
50 [15] H. Ming-Yuan, J.W. Hutchinson, *Int. J. Solids Struct.* **1989**, 25, 1053.
51
52
53
54
55
56
57
58
59
60
61
62
63
64
65

- 1
2
3
4 [16] M.Y. He, A.G. Evans, J.W. Hutchinson, *Int. J. Solids Struct.* **1994**, *31*, 3443.
5
6
7 [17] G. Noselli, V.S. Deshpande, N.A. Fleck, *Int. J. Fract.* **2013**, *183*, 241.
8
9
10 [18] C. L. Salinas, E. E. de Obaldia, C. Jeong, J. Hernandez, P. Zavattieri, D. Kisailus, J.
11
12 *Mech. Behav. Biomed. Mater.* **2017**, *76*, 58.
13
14
15 [19] E. E. de Obaldia, C. Jeong, L.K. Grunenfelderb, D. Kisailus, P. Zavattieri, *J. Mech.*
16
17 *Behav. Biomed. Mater.* **2015**, *48*, 70.
18
19
20
21 [20] J. J. Biernacki, J. W. Bullard, G. Sant, K. Brown, F.P. Glasser, S. Jones, T. Ley, R.
22
23 *Livingston, L. Nicoleau, J. Olek, F. Sanchez, J. Am. Ceram. Soc.* **2017**, *100*, 2746.
24
25
26 [21] W. Gao, Y. Zhang, D. Ramanujan, K. Ramani, Y. Chen, C.B. Williams, C.C. Wang,
27
28 Y.C. Shin, S. Zhang, P.D. Zavattieri, *Comput. Aided Des.* **2015.**, *69*, 65.
29
30
31 [22] B. Zareiyan, B. Khoshnevis, *Automat. Constr.* **2017**, *81*, 112.
32
33
34 [23] G. Franchin, P. Scanferla, L. Zeffiro, H. Elsayed, A. Baliello, G. Giacomello, M.
35
36 *Pasetto, P. Colombo, J. of Eur. Ceram. Soc.* **2017**, *37*, 2481.
37
38
39
40 [24] A. Perrot, D. Rangeard, A. Pierre, *Mater. Struct.* **2016**, *49*, 1213.
41
42
43 [25] P. Shakor, J. Sanjayan, A. Nazari, S. Nejadi, *Constr. Build. Mater.* **2017**, *138*, 398.
44
45
46 [26] B. Zareiyan, B. Khoshnevis, *Automat. Constr.* **2017**, *83*, 212.
47
48
49 [27] B. Panda, S. C. Paul, M. J. Tan, *Matter. Lett.* **2017**, *209*, 146.
50
51
52 [28] S. C. Paul, Y.W. D. Tay, B. Panda, M. J. Tan, *Arch. Civ. Mech. Eng.* **2018**, *18*, 311.
53
54
55
56
57
58
59
60
61
62
63
64
65

- 1
2
3
4 [29] T. T. Le, S. A. Austin, S. Lim, R. A. Buswell, R. Law, A. GF. Gibb, T. Thorpe,
5
6 Cement. Concrete. Res. **2012**, 42, 558.
7
8
9
10 [30] P. Shakor, J. Sanjayan, A. Nazari, S. Nejadi, Constr. Build. Mater. **2017**, 138, 398.
11
12
13 [31] D. D. Higgins, J. E. Bailey, J. Mater. Sci. **1976**, 11, 1995.
14
15
16 [32] N. B. Eden, J. E. Bailey, J. Mater. Sci. **1984**, 19, 150.
17
18
19 [33] L. J. Struble, P.E. Stutzman, E.R. Fuller, J. Am. Ceram. Soc., **1989**, 72, 2295.
20
21
22 [34] M. Hambach, D. Volkmer, Cem. Concr. Compos. **2017**, 79, 62.
23
24
25 [35] P. Feng, X. Meng, J.F. Chen, L. Ye, Constr. Build. Mater. **2015**, 93, 486.
26
27
28 [36] L. J. Struble, P.E. Stutzman, E.R. Fuller, J. Am. Ceram. Soc., **1989**, 72, 2295.
29
30
31 [37] Harsh, S., Shen, Z. and Darwin, D., 1990. Strain-Rate Sensitive Behavior of Cement
32
33 Paste and Mortar in Compression.
34
35
36 [38] V.C. Li, M. Maalej, Y-M. Lim, in *Fracture of Brittle Disordered Materials: Concrete,*
37
38 *Rock and Ceramics* (Eds: G. Baker, B. L. Karihaloo), CRC Press. **2004**, Part 2.
39
40
41 [39] J.C. Weaver, G.W. Milliron, A. Miserez, K. Evans-Lutterodt, S. Herrera, I. Gallana,
42
43 W.J. Mershon, B. Swanson, P. Zavattieri, E. DiMasi, D. Kisailus, **2012**. Sci. 336, 1275.
44
45
46 [40] Suksangpanya, N., Doctoral Thesis, Purdue University, December, **2016**.
47
48
49
50 [41] N. Suksangpanya, N. A. Yaraghi, D. Kisailus, P. Zavattieri, J. Mech. Behav. Biomed.
51
52 Mater. **2017**, 76, 38.
53
54
55
56
57
58
59
60
61
62
63
64
65

- 1
2
3
4 [42] N. Suksangpanya, N. A. Yaraghi, R. B. Pipes, D. Kisailus, P. Zavattieri, *Int. J. Solids*
5
6
7 *Structs.* **2018**, in review.
8
9
10 [43] Chen, X., Wu, S. and Zhou, J., *Constr. Build. Mater.* **2013**, *40*, 869.
11
12
13 [44] ASTM C150 – 17, Standard Specification for Portland Cement.
14
15
16 [45] ASTM C494 – 16, Standard Specification for Chemical Admixtures for Concrete.
17
18
19 [46] M. Moini, *Master's thesis*, University of Wisconsin-Milwaukee, August, **2015**.
20
21
22 [47] ASTM C1161 – 13, Standard Test Method for Flexural Strength of Advanced
23
24
25 *Ceramics at Ambient Temperature*.
26
27
28 [48] A. Börger, P. Supancic, R. Danzer, *J. of Eur. Ceram. Soc.* **2002**, *22*, 1425.
29
30
31 [49] A. Börger, P. Supancic, R. Danzer, *J. of Eur. Ceram. Soc.* **2004**, *24*, 2917.
32
33
34 [50] Y. Cao, P. Zaverri, J. Youngblood, R. Moon, J. Weiss, *Cem. Concr. Compos.*
35
36 **2015**, *56*, 73.
37
38
39 [51] J.S. Magdeski, *J. Univ. Chem. Technol. Metall.* **2010**. *45*, 143.
40
41
42 [52] L.F. Nielsen, *J. Am. Ceram. Soc.* **1990**, *73*, 2684.
43
44
45
46
47
48
49
50
51
52
53
54
55
56
57
58
59
60
61
62
63
64
65

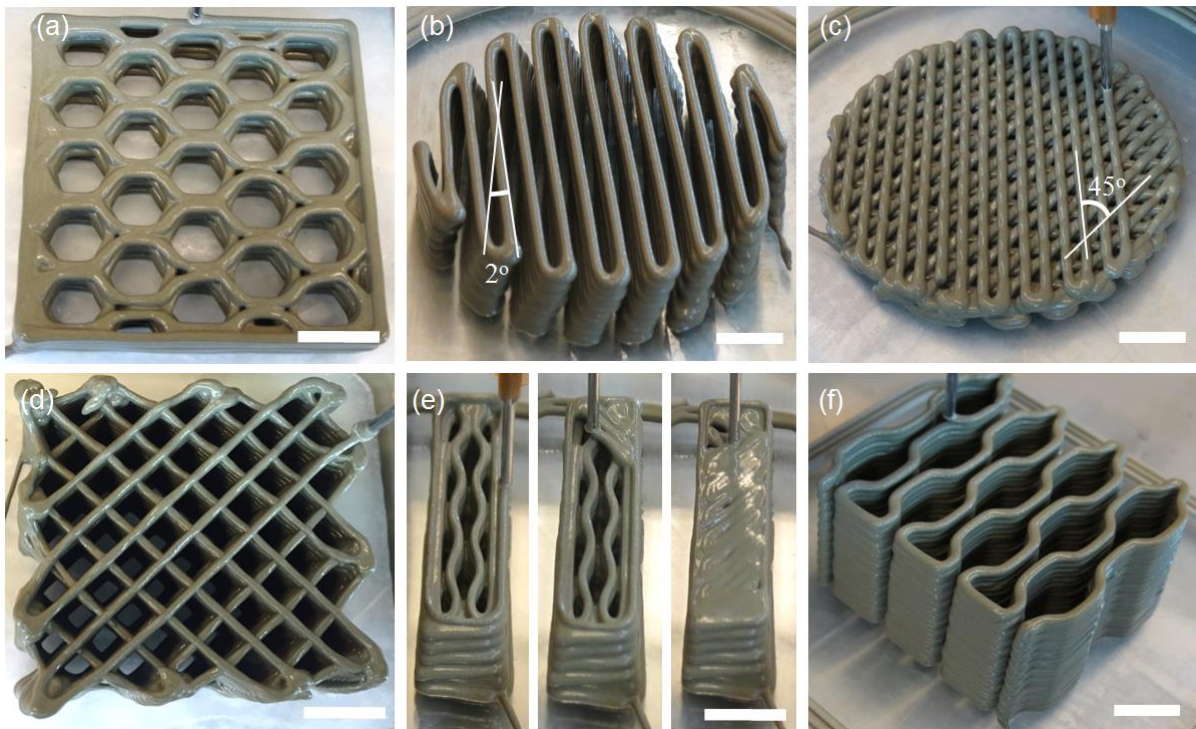


Figure 1. Various 3D printed architectures of hardened cement paste (hcp) elements: a) Closed cell honeycomb architecture; b-c) Bouligand architecture with, respectively, pitch angle $\gamma = 2^\circ$ and 45° ; d) Grid structure; e) Closed face sandwich panel beams with two solid layers at the top and bottom. f) Compliant structure with honeycomb architecture. All scale bars are 10.0 mm.

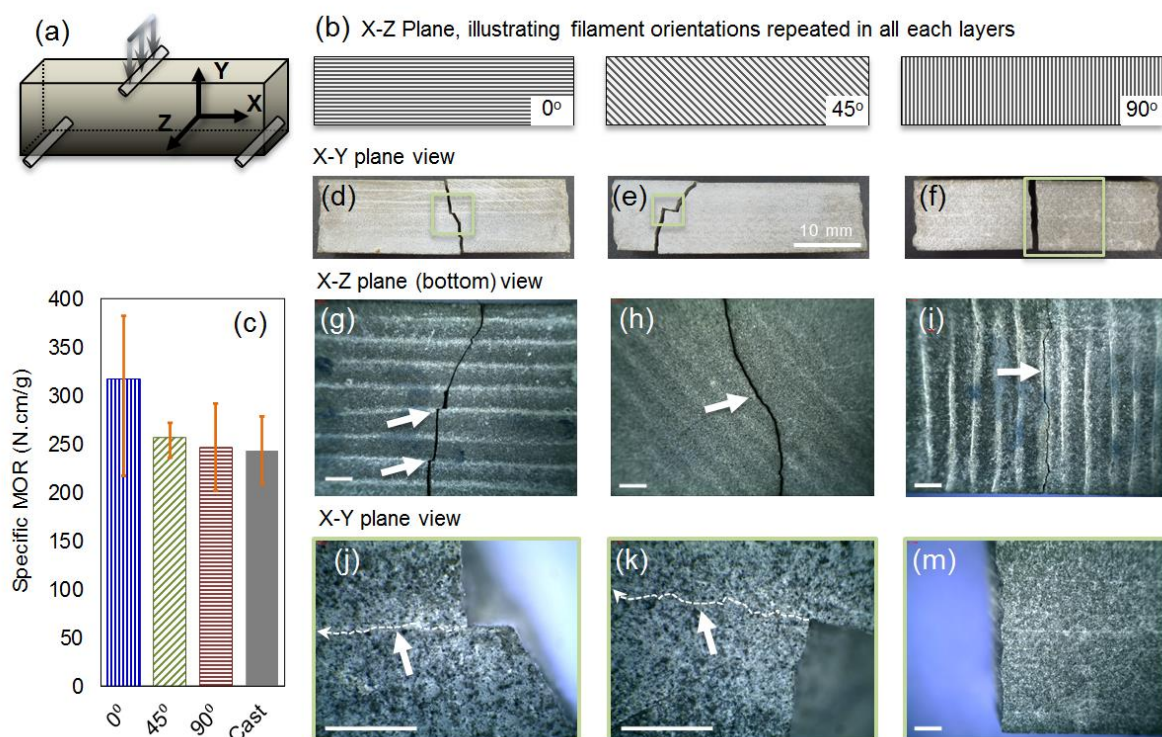


Figure 2. Mechanical response of 3D printed solid prisms with various architectures tested in 3PB: a) Schematic of the 3PB test illustrating orientation of the X,Y,Z axes b) Schematic of architectures plane view with orientation of the filaments repeated in all layers in X-Y c) Specific modulus of rupture of 3D printed elements with 0°, 45°, and 90° filament orientation versus cast specimens, d-i) Images of 0°, 45° and 90° specimens after failure illustrating crack patterns in X-Y plane view, g-i) X-Z plane (bottom) view, and j-m) micro-cracks in X-Y plane view in 0°, 45° prisms. All scale bars are 1.50 mm unless indicated.

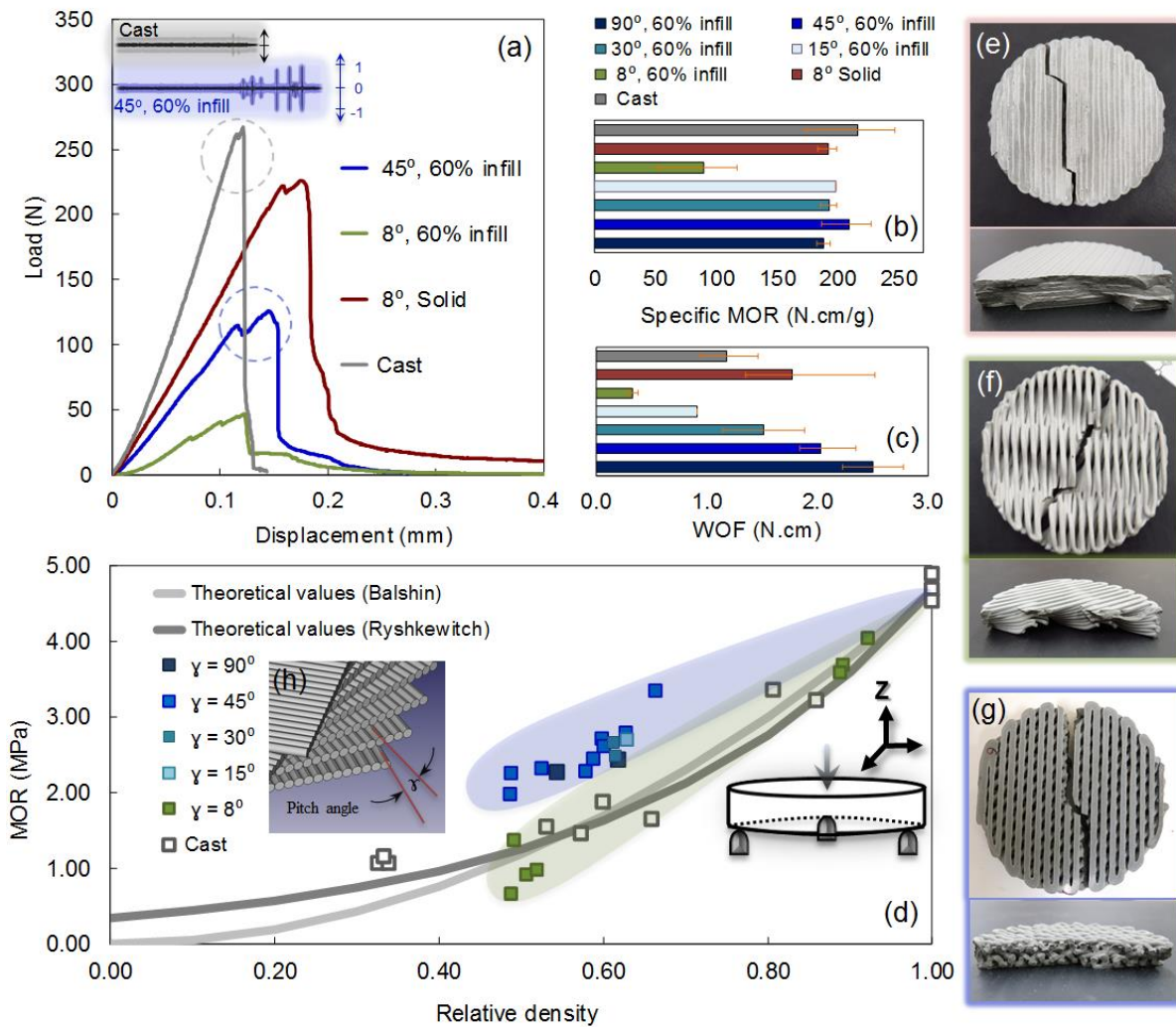
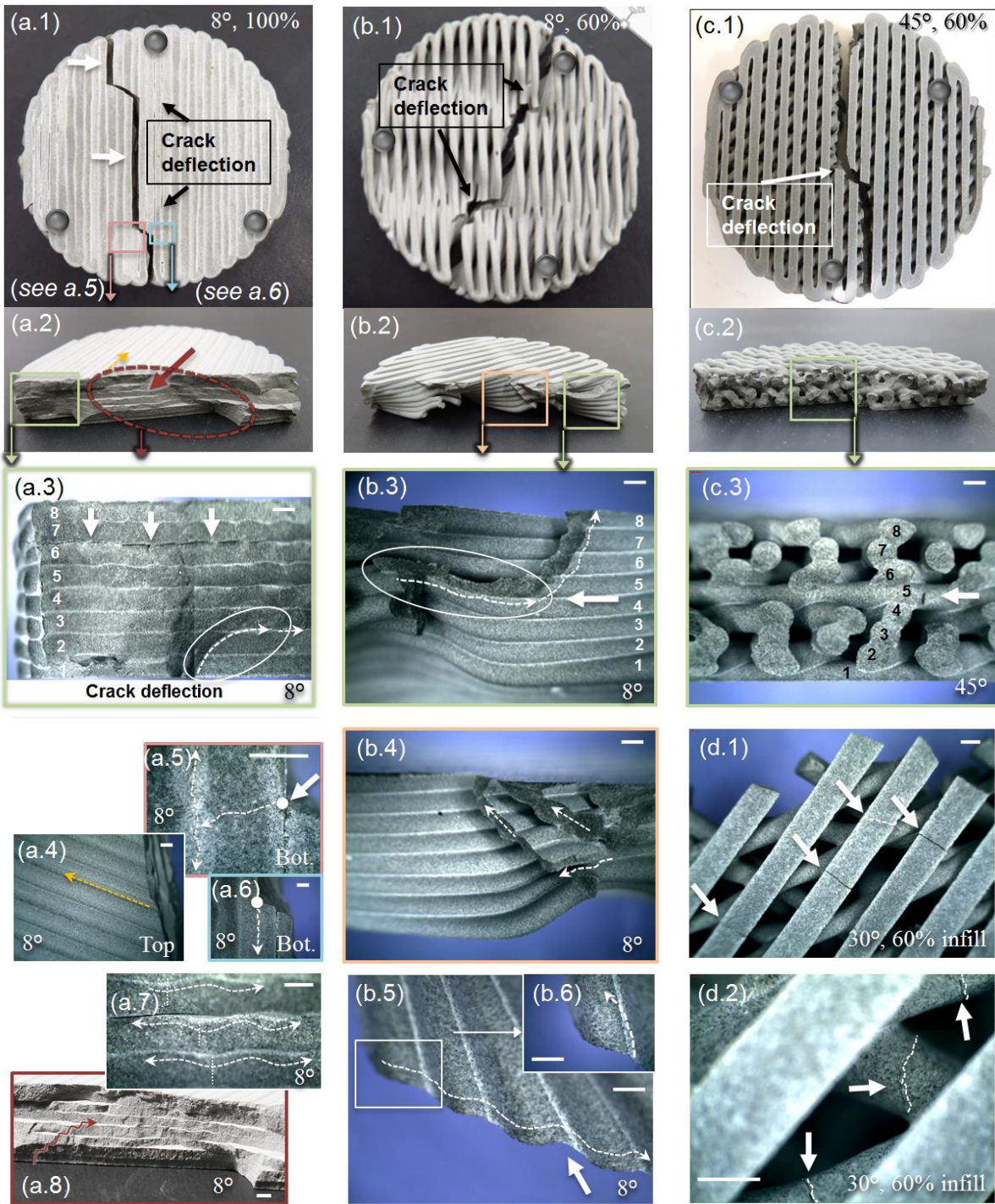


Figure 3. Mechanical response of Bouligand architecture using Ball-on-three-balls test. a) Load-displacement for printed disc specimens versus conventional cast controls, including screen shot of acoustic recording during testing. b) Specific modulus of rupture, c) Work of fracture, and d) Modulus of rupture versus relative density for Bouligand architectures with varying pitch angle ($\gamma=8^\circ, 15^\circ, 30^\circ, 45^\circ, 90^\circ$) and percentage of infill (60% and 100%) compared to cast control discs, printed Bouligand architectures with e) $\gamma=8^\circ$ with 100% infill f) $\gamma=8^\circ$ with 60% infill g) $\gamma=45^\circ$ with 100% infill.



1
2
3
4 **Figure 4.** Crack paths and fracture patterns of various 3D printed Bouligand architectures: a1-
5
6 a8) $\gamma = 8^\circ$, 100% infill, b1-b6) $\gamma = 8^\circ$, 60% infill, c1-c3) $\gamma = 45^\circ$, 60% infill, and d1,d2) $\gamma =$
7
8 30°, 60% infill after B3B test. All scale bars are 1.0 mm.
9
10
11
12
13
14
15
16
17
18
19
20
21
22
23
24
25
26
27
28
29
30
31
32
33
34
35
36
37
38
39
40
41
42
43
44
45
46
47
48
49
50
51
52
53
54
55
56
57
58
59
60
61
62
63
64
65

Supporting Information

Additive Manufacturing and Performance of Architected Cement-based Materials

*Mohamadreza Moini, Jan Olek, Jeffrey Youngblood, Bryan Magee, Pablo D. Zavattieri**

A honeycomb architecture with close cell (**Figure S1a**) and open cell (compliant) design (**Figure S1b**) is demonstrated. The compliant structure can demonstrate bilinear stress-strain behavior, including a primary linear strain recovery ($E1$) at strains below which the layered filaments make contact (cycles 1-5 in **Figure S1c1**) and a secondary linear response above strains ($E2$) at which the filament's contact take place (cycles 6 in **Figure S1c1**). As can be seen, the jointless compliant structure shown, exhibits two discrete moduli ($E1$, $E2$) depending on whether the filaments have made contact (**Figure S1d,e**) or not (**Figure S1f,g**). In contrast, the closed cell honeycomb architecture (HC) and cast element exhibit only one value of modulus (**Figure S1c2**). This dual response can be customized as applicable with suitable design of the architecture, spacing between filaments, and material property. The cast element represents a strain at failure of about 0.008. This is in the general range reported for typical hardened cement paste ^[31]. In complaint structure, in addition to the bi-linear response, a strain (as high as 0.025 in the bi-linear region) much higher than the strain at failure commonly observed for cast hardened cement paste (0.005 to 0.008) ^[31] is exhibited.

Video 1-4: Bouligand architecture with 15°, 30°, 45°, 90° pitch angle

Video 5,6: Two typical compliant structure

Video 7-9: Sandwich panel beams with closed top and bottom face

Video 10: Grid structure

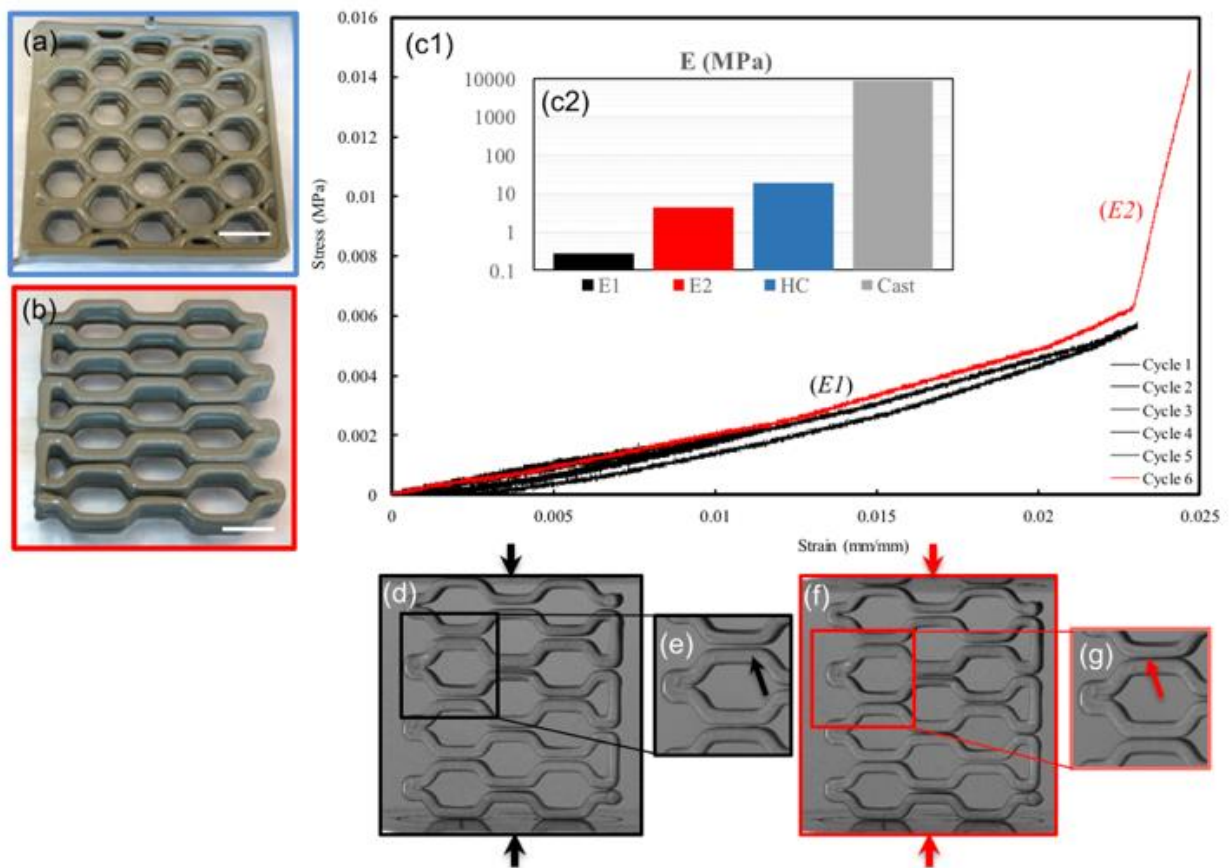
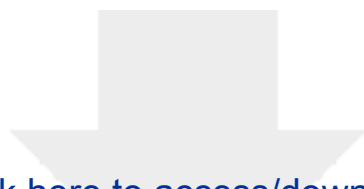


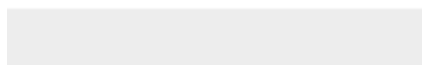
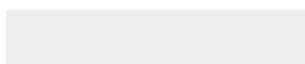
Figure S1. a) Closed cell honeycomb structure. b) Compliant structure with honeycomb architecture. c) Bilinear stress-strain behavior including five primary linear strain recovery (Cycles 1-5) and secondary response (Cycle 6) before and after filament's contact. c-i) Comparison of two discrete moduli of elasticity of compliant structure ($E1, E2$) with closed cell honeycomb and cast. d,e) Compliant structure in cyclic loading (cycles 1-5) prior to filament's contact. f,g) Compliant structure after filament's contact takes place.

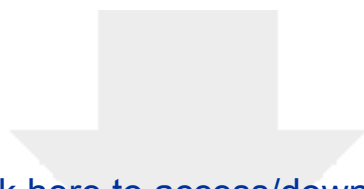


Click here to access/download

Supporting Information

Vid 1. Bouligand, 15 Deg..mp4

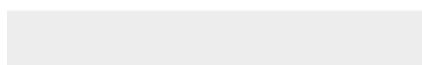
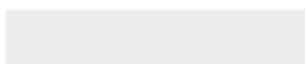




Click here to access/download

Supporting Information

Vid 2. Bouligand, 30 Deg..mp4





Click here to access/download

Supporting Information

Vid 3. Bouligand, 45 Deg..mp4

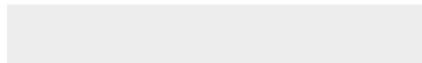




[Click here to access/download](#)

Supporting Information

Vid 4. Bouligand, 90 Deg..mp4

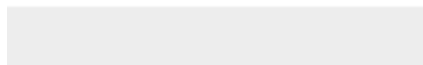




Click here to access/download

Supporting Information

Vid 5. Compliant Structure 1.mp4





Click here to access/download

Supporting Information

Vid 6. Compliant Structure 2.mp4





Click here to access/download

Supporting Information

Vid 7. Sandwich Panel 1.mp4

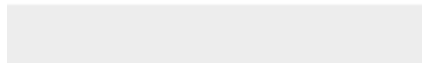




Click here to access/download

Supporting Information

Vid 8. Sandwich Panel 2.mp4

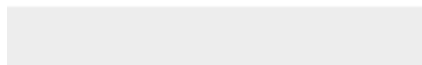
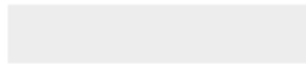




Click here to access/download

Supporting Information

Vid 9. Sandwich Panel 3.mp4





Click here to access/download
Supporting Information
Vid 10. Grid Structure.mp4

